INTERNATIONAL JOURNAL FOR NUMERICAL METHODS IN FLUIDS
*Int. J. Numer. Meth. Fluids* 2008; **56**:1155–1160
Published online 20 December 2007 in Wiley InterScience (www.interscience.wiley.com). DOI: 10.1002/fld.1710

# The numerical prediction of droplet deformation and break-up using the Godunov marker-particle projection scheme

F. Bierbrauer and T. N. Phillips*, †

*School of Mathematics, Cardiff University, Senghennydd Road, Cardiff CF24 4AG, U.K.*

SUMMARY

The problem of droplet deformation and break-up is considered. A hybrid Eulerian–Lagrangian method is used in which the velocity and pressure are discretized on a fixed mesh and Lagrangian particles are used to implicitly track the interface between the two phases. The Navier–Stokes equations are solved using an approximate Godunov projection method, collectively called the Godunov marker-particle projection scheme. The results show good qualitative agreement with previous research as well as demonstrating the efficacy of the method. Copyright © 2007 John Wiley & Sons, Ltd.

Received 11 April 2007; Revised 6 November 2007; Accepted 7 November 2007

KEY WORDS: droplet deformation; surface tension; second-order Godunov scheme; projection method

## 1. INTRODUCTION

An understanding of the break-up of fluid droplets is important in a wide variety of industrial, engineering and natural processes. Typically, such two-fluid processes range over microscopic to macroscopic scales. Microscopic droplet formation and manipulation are important processes in DNA analysis, protein crystallization, analysis of human physiological fluids, ink jet printing and chemical processing. At larger scales, droplet dynamics play a role in the automotive industry such as in fuel sprays and fuel injection systems.

The droplet break-up process is governed by the interplay of viscous and inertial forces, tending to deform the droplet, and capillary forces that attempt to restore deformed droplets to an equilibrium shape. Experimental studies [1] have shown that the break-up process is governed by the

*Correspondence to: T. N. Phillips, School of Mathematics, Cardiff University, Senghennydd Road, Cardiff CF24 4AG, U.K.
†E-mail: phillipstn@cf.ac.uk

Contract/grant sponsor: EPSRC

Ohnesorge number, $Oh=\mu_d/\sqrt{\rho_d D_0 \sigma_{ad}}$, which reflects the effect of droplet viscosity on droplet break-up, although viscous effects play no role when $Oh<0.1$ [2]. In addition, the droplet break-up regimes are characterized by the initial Weber number, $We_i=\rho_a D_0 U_0^2/\sigma_{ad}$, which represents the ratio of disruptive hydrodynamic force to stabilizing force. Observations indicate that there are three distinct mechanisms of droplet break-up: droplet deformation, boundary layer stripping and surface disturbances caused by the Kelvin–Helmholtz and Rayleigh–Taylor instabilities [3]. The various break-up modes are defined as vibrational ($We_i \leqslant 12$), bag ($12<We_i \leqslant 50$), bag-and-stamen break-up ($50<We_i \leqslant 100$) as well as sheet stripping ($100<We_i \leqslant 350$) and catastrophic break-up ($We_i>350$) [2].

A simplified two-dimensional, incompressible fluid dynamical model of a translating fluid droplet (d), of density $\rho_d$, viscosity $\mu_d$, initial droplet diameter $D_0$, surface tension coefficient $\sigma_{ad}$ and initial relative velocity $U_0$, immersed in an immiscible, ambient (a) fluid, of density $\rho_a$ and viscosity $\mu_a$, is used in this paper. While some aspects of droplet break-up are a three-dimensional phenomenon, a two-dimensional simulation can still provide a good deal of insight into the break-up process and may be qualitatively compared with experimental results [3, 4]. Although the structure of fluid interfaces is a complex molecular process, the macroscopic properties of interfacial flow can be adequately captured through use of surface force models. One such model, that of Brackbill *et al.* [5], will be used in this paper.

The numerical solution of two-phase flow problems remains a difficult task. Such a numerical method must be able to accurately track multiple fluid interfaces while maintaining stability in the presence of density discontinuities and, in the case of incompressible fluids, ensuring a solenoidal velocity field. Typically, Eulerian-fixed grid methods, such as VOF, possess the advantage of allowing multiple fluid interfaces to undergo large deformation without loss of accuracy, although making the calculation of the interface itself inaccurate. Lagrangian methods, on the other hand, while being able to accurately determine material interfaces, suffer from the generation of distorted meshes for strong interfacial deformation. A hybrid Eulerian–Lagrangian method, where the advection of fluid phase is handled in a Lagrangian manner while fluid velocity and pressure information is constructed on a fixed Eulerian grid, makes use of both approaches.

One such method, the Godunov marker-particle projection scheme (GMPPS) [6], has been used to simulate two-phase flows such as a water droplet falling into a pool of water [7] as well as the impact of a fluid droplet onto a solid surface [8]. It possesses several advantages over older methods such as VOF or the MAC method. The method is inherently second-order accurate in time and space using an approximate projection method as well as Godunov upwinding to deal with high Reynolds number flows [9], an improvement on the first-order accuracy of the MAC method. In addition, permanently assigned marker particles are used to transport fluid phase information avoiding the artificial smoothing prevalent in VOF methods [6]. The method has not yet been used to model the droplet break-up process. The main aim of this paper is to examine the performance of the GMPPS for such problems.

## 2. GOVERNING EQUATIONS

We consider a one-field formulation of the governing equations for unsteady incompressible flow. The Navier–Stokes equations are solved in the domain $\Omega=\{(x, y): 0<x<X,\ 0<y<Y\}$. Thus, for



DOI: 10.1002/fld

two-phase flow, the governing equations expressed in dimensionless form are

$$\begin{aligned}
\frac{\partial \mathbf{u}}{\partial t}+(\mathbf{u}\cdot\nabla)\mathbf{u} &= -\frac{1}{\rho}\nabla p+\frac{1}{\rho Re}\nabla\cdot\mu(\nabla\mathbf{u}+(\nabla\mathbf{u})^{\mathrm{T}})+\frac{\kappa(\mathbf{x})\nabla\rho}{We[\rho]\langle\rho\rangle}\\
\nabla\cdot\mathbf{u} &= 0\\
\frac{\partial C}{\partial t}+\mathbf{u}\cdot\nabla C &= 0\\
\rho &= C+(1-C)\rho_{\mathrm{ad}}\\
\mu &= (C+(1-C)/\mu_{\mathrm{ad}})^{-1}
\end{aligned} \tag{1}$$

where we have non-dimensionalized length with respect to $D_0$, velocity with respect to $U_0$, density with respect to $\rho_{\mathrm{d}}$, viscosity with respect to $\mu_{\mathrm{d}}$, pressure with respect to $\rho_{\mathrm{d}}U_0^2$ and the convective time with respect to $D_0/U_0$. The Reynolds number is defined by $Re=\rho_{\mathrm{d}}U_0D_0/\mu_{\mathrm{d}}$ and we have used $\rho_{\mathrm{ad}}=\rho_{\mathrm{a}}/\rho_{\mathrm{d}}$, $\mu_{\mathrm{ad}}=\mu_{\mathrm{a}}/\mu_{\mathrm{d}}$. The volume fraction $C=C_{\mathrm{d}}$ so that $C_{\mathrm{a}}=1-C_{\mathrm{d}}$. The surface force term is expressed through the curvature $\kappa(\mathbf{x})=\nabla\cdot\mathbf{n}$ where $\mathbf{n}=\nabla\rho/|\nabla\rho|$ is the normal to the interface, the jump in density across the interface is $[\rho]=1-\rho_{\mathrm{ad}}$ and average of the densities is given by $\langle\rho\rangle=(1+\rho_{\mathrm{ad}})/2$.

Boundary conditions are a specified constant velocity, $\mathbf{u}(0,y,t)=\mathbf{i}$, on the inflow boundary of the domain, whereas we use the free boundary conditions, considered as streamlines, of Jin and Braza [10] on the upper and lower boundaries: $\partial u(x,0;Y,t)/\partial y=0$, $v(x,0;Y,t)=0$. Zhu [11] argues that the boundary conditions at outflow should be $\partial\mathbf{u}(X,y,t)/\partial n=0$ and we have adopted this condition. No flux conditions on the density, viscosity and consequently the volume fraction are used for all boundaries, i.e. $\mathbf{n}\cdot\nabla\rho|_{\partial\Omega}=\mathbf{n}\cdot\nabla\mu|_{\partial\Omega}=\mathbf{n}\cdot\nabla C|_{\partial\Omega}=0$. Note that the flow is fully two-dimensional without use of symmetry conditions along the plane of symmetry.

Although no pressure boundary conditions are required, projection methods make use of a gauge variable $\phi$ to ensure satisfaction of an approximate solenoidal velocity field. All gauge variable boundary conditions are homogeneous Neumann conditions: $\mathbf{n}\cdot\nabla\phi|_{\partial\Omega}=0$ except at the outflow boundary where Zhu [11] recommends $\partial\phi/\partial\tau=0$. This last condition may be integrated along the outflow part of the boundary to yield $\phi=$constant. The condition $\phi(X,y,t)=0$ at outflow is sometimes implemented in the literature.

Initial densities and viscosities were constant in each fluid and all initial pressures were zero. Initially, we prescribe $\mathbf{u}^0=\mathbf{i}$ in the ambient fluid and $\mathbf{u}^0=\mathbf{0}$ in the droplet.

## 3. GODUNOV MARKER-PARTICLE PROJECTION SCHEME

System (1) is solved using the approximate Godunov projection method [9] with second-order Crank–Nicolson time discretization. Given the strengths and weaknesses of the various projection methods, we choose to use a modified version of the incremental pressure projection method of Rider *et al.* [7]. The original method uses a time-lagged discretization of the pressure gradient in the momentum equation, sets the intermediate velocity boundary conditions to the physical boundary conditions and uses a homogeneous Neumann condition in the projection stage of the algorithm. The modification to this method uses a corrected pressure update to ensure consistency and incorporates a variable density.



DOI: 10.1002/fld

In semi-discrete form, this results in the following pressure-corrected, variable density, second-order approximation of the equations in (1) at time $t^n$:

1. *Step 1*: Given $\mathbf{u}^n$, $\nabla p^{n-1/2}$, $\rho^n$, $\mu^n$, $C^n$ calculate $(\mathbf{u}\cdot\nabla\mathbf{u})^{n+1/2}$.
2. *Step 2*: update $C^{n+1}$ so that

$$\rho^{n+1}=C^{n+1}+(1-C^{n+1})\rho_{\mathrm{ad}},\quad \mu^{n+1}=(C^{n+1}+(1-C^{n+1})/\mu_{\mathrm{ad}})^{-1}\quad \text{in } \Omega$$

   so that $\rho^{n+1/2}=(\rho^n+\rho^{n+1})/2$ and $\mu^{n+1/2}=(\mu^n+\mu^{n+1})/2$.
3. *Step 3*: solve for the intermediate velocity:

$$\left(\mathbf{I}-\frac{\Delta t}{2Re}\sigma^{n+1/2}L_\mu^{n+1/2}\right)\mathbf{u}^*=\left(\mathbf{I}+\frac{\Delta t}{2Re}\sigma^{n+1/2}L_\mu^{n+1/2}\right)\mathbf{u}^n$$
$$-(\Delta t((\mathbf{u}\cdot\nabla\mathbf{u})^{n+1/2}+\sigma^{n+1/2}\nabla p^{n-1/2}-\sigma^{n+1/2}\mathbf{F}_v^{n+1/2})\quad \text{in } \Omega \tag{2}$$

4. *Step 4*: project the result:

$$L_\sigma^{n+1/2}\phi^{n+1}=\frac{1}{\Delta t}\nabla\cdot\mathbf{u}^*\quad \text{in } \Omega \tag{3}$$

   followed by

$$\mathbf{u}^{n+1}=\mathbf{u}^*-\Delta t\sigma^{n+1/2}\nabla\phi^{n+1}\quad \text{in } \bar{\Omega} \tag{4}$$

5. *Step 5*: update the pressure gradient:

$$\nabla p^{n+1/2}=\nabla p^{n-1/2}+\nabla\phi^{n+1}-\frac{\Delta t}{2Re}L_\mu^{n+1/2}(\sigma^{n+1/2}\nabla\phi^{n+1})\quad \text{in } \bar{\Omega} \tag{5}$$

where $\mathbf{F}_v=\kappa(\mathbf{x})\rho\nabla\rho/We[\rho]\langle\rho\rangle$ and the Laplacian operators are given by $L_\mu\mathbf{w}=\nabla\cdot\mu(\nabla\mathbf{w}+(\nabla\mathbf{w})^{\mathrm{T}})$, for some vector $\mathbf{w}$, and $L_\sigma\psi=\nabla\cdot\sigma\nabla\psi$, for some scalar $\psi$, $\sigma=1/\rho$, $\sigma^{n+1/2}=(\sigma^n+\sigma^{n+1})/2$ and $\bar{\Omega}=\Omega\cup\partial\Omega$. The $(\mathbf{u}\cdot\nabla\mathbf{u})^{n+1/2}$ term represents an approximation to the nonlinear advection term at the half time level and is the one detailed in [9]. The velocity at the half-time level has also been used in the viscous term and is given by $\mathbf{u}^{n+1/2}=(\mathbf{u}^n+\mathbf{u}^*)/2$. The extra pressure correction term $-(\Delta t/2Re)L_\mu\sigma\nabla\phi$ was obtained by eliminating the intermediate velocity in the momentum equation (2) using the update given by (4).

Note that in the projection method described above, the time-updated density and viscosity are required in Step 1 where only the values at the $n$th time level are known. This is calculated with the use of the GMPPS [6] where fluid particles are advanced forward in time to track individual fluid phases while carrying particle colour information. The time-updated volume fraction for the fluid phase $C^{n+1}$ is then obtained by interpolation from surrounding fluid particles of that phase. This provides the solution of the advection equation for the volume fraction.

Since there are discontinuities in the physical properties, such as density and viscosity, an element of smoothing is necessary. In practice, the volume fraction is smoothed by forming the convolution of $C$ with a kernel $K(\mathbf{x};\varepsilon)$ that becomes the surface delta function as $\varepsilon\to 0$ [8].



DOI: 10.1002/fld

## 4. NUMERICAL RESULTS

Tests of the GMPPS method have been performed elsewhere, see [6, 8], and will not be repeated here. The following droplet break-up simulations were performed on a non-dimensionalized computational domain of five times the initial droplet diameter, as used in [3, 4], in each direction with a $128^2$ grid. Each simulation shows the deformation of a droplet with: $\rho_d = 9200\,\mathrm{kg/m^3}$, $D_0 = 9\,\mathrm{mm}$, $\mu_d = 2.82 \times 10^{-4}\,\mathrm{Pa\,s}$ within an ambient medium: $\rho_a = 996\,\mathrm{kg/m^3}$, $\mu_a = 8.54 \times 10^{-4}\,\mathrm{Pa\,s}$ and an interfacial surface tension coefficient of $\sigma_{ad} = 0.4\,\mathrm{N/m}$. For all the simulations presented the Ohnesorge number $Oh = 5 \times 10^{-5}$. Since $Oh < 0.1$, viscous effects play a negligible role. The Weber number was varied through three different initial relative velocities $U_0 = 0.73, 0.82$ and $2.12\,\mathrm{m/s}$ corresponding to $We = 12, 15$ and 100; these results are shown in Figures 1–3.

These Weber numbers were chosen to allow a comparison to the results of Duan *et al.* [3]: $We = 12, 15$ and Zaleski *et al.* [4]: $We = 100$. The results for the $We = 12, 15$ cases show good qualitative agreement, although the present results are more detailed and relate better to the $We = 10$ result of Zaleski *et al.* [4]. The detailed break-up mechanism of the $We = 100$, $t = 0.019\,\mathrm{s}$ result shows qualitative similarity to the equivalent simulation of [4], which is the start of the sheet

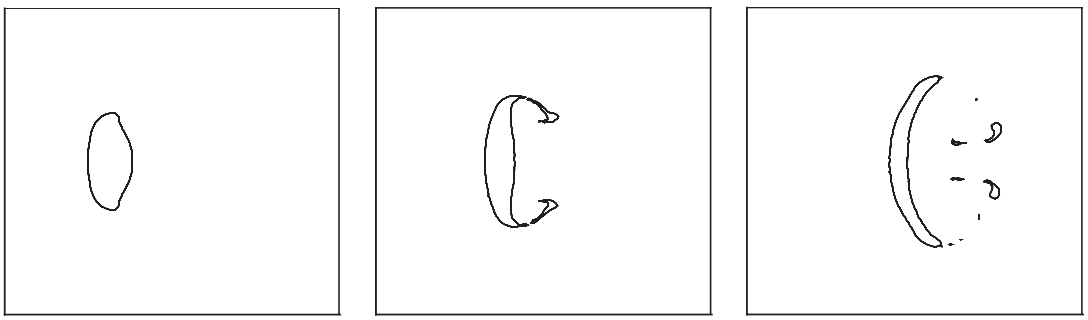


Figure 1. Droplet break-up simulations for an initial Weber number of $We_i = 12$.

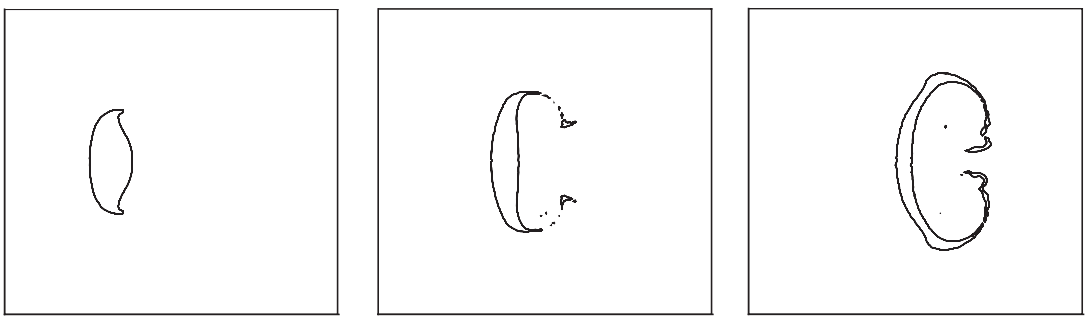


Figure 2. Droplet break-up simulations for an initial Weber number of $We_i = 15$.



DOI: 10.1002/fld

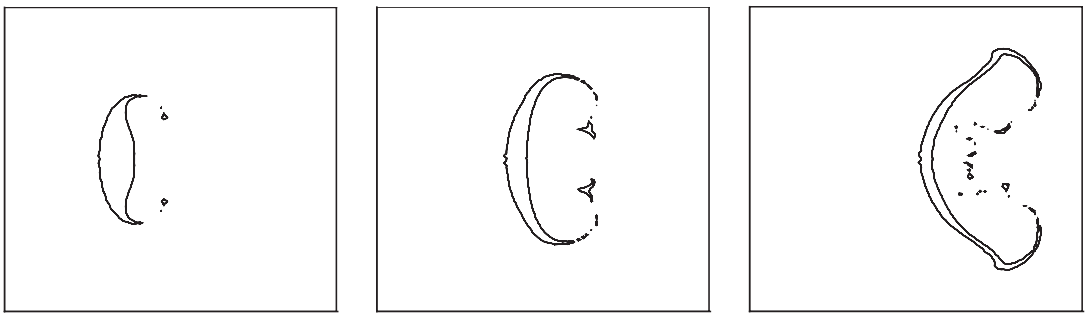

$t = 0.0095$ s $t = 0.014$ s $t = 0.019$ s

Figure 3. Droplet break-up simulations for an initial Weber number of $We_i = 100$.

stripping regime. Note that the drawn-out arms of the droplet seen in Figure 2 for $We = 15 : t = 0.037, 0.05$ s and in Figure 3 for $We = 100 : t = 0.014, 0.019$ s curve inward towards the droplet; this is a consequence of the chosen boundary conditions. In addition, although simulated results of the $We = 12, 15$ cases are representations of experimentally obtained bag break-up, they show sheet stripping, such mechanisms are not expected to become obvious unless much higher grid resolutions are used [4]. It is also evident from the present simulations that the flow demonstrates clear symmetry about a line drawn through the centre of the droplet indicating the ability of the method to maintain the symmetry inherent to the problem. It is clear that the GMPP scheme may be used to simulate the droplet break-up mechanism and should provide better approximations for higher grid resolution and an extension to three dimensions.

## REFERENCES


1. Hinze JO. Fundamentals of the hydrodynamic mechanism of splitting in dispersion processes. *AIChE Journal* 1955; **1**:289–295.
2. Nomura K, Koshizuka S, Oka Y, Obata H. Numerical analysis of droplet breakup behavior using particle method. *Journal of Nuclear Science and Technology* 2001; **38**:1057–1064.
3. Duan RQ, Koshizuka S, Oka Y. Numerical and theoretical investigation of effect of density ratio on the critical Weber number of droplet breakup. *Journal of Nuclear Science and Technology* 2003; **40**:501–508.
4. Zaleski S, Li J, Succi S. Two-dimensional Navier–Stokes simulation of deformation and breakup of liquid patches. *Physical Review Letters* 1995; **75**:244–247.
5. Brackbill JU, Kothe DB, Zemach A. A continuum model for modeling surface tension. *Journal of Computational Physics* 1992; **100**:335–354.
6. Bierbrauer F, Zhu S-P. A numerical model for multiphase flow based on the GMPPS formulation, part I: kinematics. *Computers and Fluids* 2007; **36**:1199–1212.
7. Rider WJ, Kothe DB, Mosso SJ, Cerutti JH, Hochstein JI. Accurate solution algorithms for incompressible multiphase flows. *AIAA Report 95-0699*, *33rd Aerospace Sciences Meeting*, Reno, NV, 1995.
8. Bierbrauer F. Mathematical modelling of water-droplet impact on hot galvanised steel surfaces. *Ph.D. Thesis*, University of Wollongong, 2004.
9. Puckett EG, Almgren A, Bell JB, Marcus DL, Rider WJ. A high-order projection method for tracking fluid interfaces in variable density incompressible flows. *Journal of Computational Physics* 1997; **130**:269–282.
10. Jin G, Braza M. A nonreflecting outlet boundary condition for incompressible unsteady Navier–Stokes calculations. *Journal of Computational Physics* 1993; **107**:239–253.
11. Zhu J. The second-order projection method for the backward-facing step flow. *Journal of Computational Physics* 1995; **117**:318–331.




DOI: 10.1002/fld